Physics in Medicine & Biology

LETTER

To cite this article: Mingxin Jin *et al* 2018 *Phys. Med. Biol.* **63** 17LT01

View the article online for updates and enhancements.

This content was downloaded from IP address 202.120.14.158 on 29/08/2018 at 15:16

IOP Publishing Phys. Med. Biol. 63 (2018) 17LT01 (6pp) https://doi.org/10.1088/1361-6560/aad8e0

Physics in Medicine & Biology

IPEM Institute of Physics and Engineering in Medicine

LETTER

Low-rank and sparse decomposition with spatially adaptive filtering for sequential segmentation of 2D+t vessels

Mingxin Jin[1], **Dongdong Hao**[1], **Song Ding**[2] and **Binjie Qin**[1]

[1] School of Biomedical Engineering, Shanghai Jiao Tong University, Shanghai 200240, People's Republic of China
[2] Department of Cardiology, Ren Ji Hospital, School of Medicine, Shanghai Jiao Tong University, Shanghai 200127, People's Republic of China

E-mail: bjqin@sjtu.edu.cn **and** dingsong@renji.com

RECEIVED
10 April 2018

REVISED
11 July 2018

ACCEPTED FOR PUBLICATION
8 August 2018

PUBLISHED
29 August 2018

Keywords: x-ray coronary angiography, vessel segmentation, robust principal component analysis, radon-like filtering, local-to-global adaptive thresholding

Abstract

This letter proposes to extract contrast-filled vessels from overlapped noisy complex backgrounds in an x-ray coronary angiogram image sequence using low-rank and sparse decomposition. A refined vessel segmentation is finally achieved by implementing a radon-like feature filtering plus local-to-global adaptive thresholding to tackle the spatially varying noisy residuals in the extracted vessels. Based on real and synthetic XCA data, the experiment results demonstrate the superiority of the proposed method over the state-of-the-art methods.

1. Introduction

Sequentially segmenting contrast-filled vessels (Kirbas and Quek 2004, Lesage *et al* 2009, Moccia *et al* 2018) from an x-ray angiography (XCA) image sequence plays an essential role in various minimally invasive vascular interventions (Jin *et al* 2017, Ma *et al* 2017). The XCA image is a display of the x-ray attenuation sum along x-ray projection paths, and it contains various overlapped anatomical structures besides the contrast-filled vessels, including bones, diaphragms, and lungs. Furthermore, XCA images from low-dose x-ray imaging are seriously corrupted by spatially varying signal-dependent Poisson noises (Yu and Sun 2018, Zhu *et al* 2013), such that the XCA image has very low contrast and low SNR between the noises and the signals. Therefore, segmenting the contrast-filled 2D+t vessels from the noisy and complex backgrounds in an XCA image sequence is a challenging open problem in biomedical imaging.

Vessel segmentation is defined as a vessel/non-vessel pixel classifier to highlight the vessel outline, which can be classified into tracking-based, filter-based, model-based (Zhao *et al* 2017), graph-based (Kitamura *et al* 2016), and convolutional neural network- (Liskowski and Krawiec 2016) based methods. However, most methods segmented the vessels from 3D computed tomography angiography, magnetic resonance angiography or a single 2D image (Liskowski and Krawiec 2016, Vostatek *et al* 2017), of which there is no serious disturbance from the overlapped noisy background structures.

Recently, robust subspace learning has become an important topic in machine learning and biomedical imaging (Shi *et al* 2017, Tang *et al* 2017). Based on the fact that an image sequence can be modeled as a sum of low-rank and sparse components in some transform domains, robust principal component analysis (RPCA) has been exploited to separate a sparse outlier or detect moving objects from biomedical image sequences. Extracting contrast-filled vessels from the XCA images (Jin *et al* 2017, Ma *et al* 2017) via RPCA has been successfully introduced for the purpose of cardiovascular disease diagnosis (Ding *et al* 2010). However, these RPCA-based image decomposition methods obtain preliminary foreground vessels with many noisy residuals.

To the best of our knowledge, this letter proposes the first work on the challenging 2D+t vessel segmentation from XCA sequences by integrating low-rank and sparse decomposition into spatially adaptive feature-preserving image filtering. Being different from the RPCA-based vessel extraction methods, the proposed method removes the spatially varying noisy residuals from the extracted contrast-filled vessels by radon-like feature-preserving filtering (Kumar *et al* 2010) and a local-to-global adaptive thresholding strategy. The refined sequential vessel segmentation is automatically achieved to preserve the contrast-filled vessel details and remove the spatially var-

© 2018 Institute of Physics and Engineering in Medicine

ying noisy residuals simultaneously. Being different from the work (Syeda-Mahmood *et al* 2012) exploiting the spatial and temporal variance in pixels to extract arteries from an XCA image, the joint feature filtering and adaptive thresholding exploit the sparse outlier of moving contrast and the low-rankness of complex backgrounds to accurately extract contrast-filled vessels. The local-to-global adaptive thresholding, instead of only Otsu thresholding in a small window, is designed to improve the spatially adaptive vessel feature-preserving filtering on the vessel images. We thus can automatically achieve the complete sequential vessel delineation without noisy background residuals, which cannot be achieved by the state-of-the-art methods.

2. Methods

2.1. Overview

The proposed method first implements a global logarithm transformation of XCA images to create an x-ray attenuation sum model for subsequent vessel/background separation. We then extract the contrast-filled vessels from the XCA images via RPCA. Spatially adaptive feature-preserving image filtering accurately removes the noisy residuals for the refined vessel segmentation.

2.2. Logarithm transformation

In x-ray imaging, the x-ray intensity in XCA is reduced exponentially by the sum of the attenuation coefficients that the x-ray passes:

$$I_{out} = I_{in} e^{-\int_d \mu dx}, \tag{1}$$

where I_{in} and I_{out} represent the intensities of the x-rays that enter into and out of the human body, respectively, where μ denotes the attenuation coefficient, and d denotes the path of the rays.

Applying the log operator on both sides of the equation, we obtain:

$$-\ln(I_{out}/I_{in}) = \int_d \mu dx. \tag{2}$$

After intensity normalization to the range $[0, 1]$, the XCA can be regarded as the normalization of the ray intensity, i.e. the ratio of I_{out} and I_{in}. We then obtain

$$-\ln(I_{image}) = -\ln(I_{out}/I_{in}) = \int_{d_1} \mu dx + \int_{d_2} \mu dx = A_V + A_B, \tag{3}$$

where A_V and A_B define the attenuation sums caused by vessels and backgrounds, respectively. Equation (3)
ums /ActualTextFEFF00A0 BDC ( )TjEMC (()Tj0 0.537 0.816 rg/GS0 gs0 Tc 0 Tw (3)Tj0 0 0 1 k/GS1 gs35.945 0 T0.0

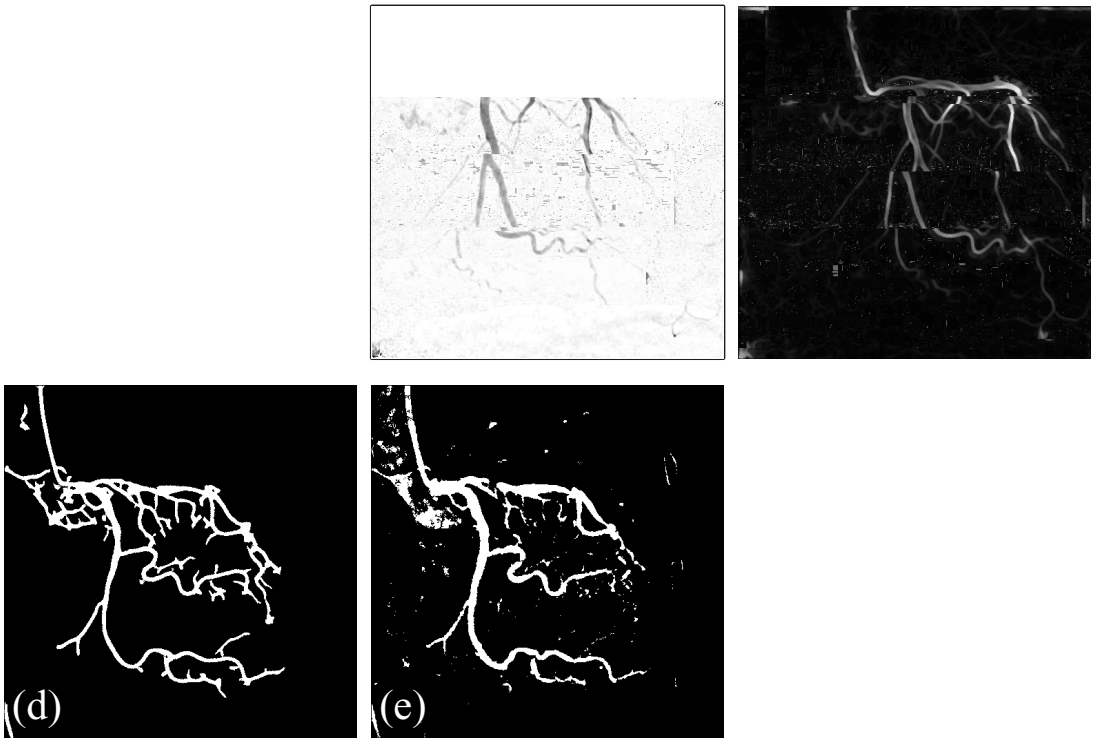

images (figure 1(a)). An example image of RLF features is shown in figure 1(c). A spatially adaptive thresholding method (Phansalkar *et al* 2011) is implemented on the RLF-filtered images to obtain binary images. This method calculates the local threshold $t_{Phansalkar}$ for each pixel based on the mean m and standard deviation s of the pixel values in a local window around this pixel using the following equation:

$$t_{Phansalkar} = m[1 + pe^{-qm} + k(\frac{s}{R} - 1)], \tag{5}$$

where p, q, k are tuning constants, and R is the dynamic range of s. The $t_{Phansalkar}$ of each pixel is calculated and a binary image is then obtained by thresholding every pixel. An example image is shown in figure 1(d). Then, regions that are too small (smaller than a fixed size t_s) are regarded as noises and thus removed from this binary image to obtain a vessel tree image.

RLF filtering thins vessels and cannot cover all the pixels in the vessels. We then apply global Otsu's thresholding (Otsu 1979) to separate the pixels of an original image into two classes by minimizing the intra-class variance, i.e.

$$t_{Otsu} = \arg\min_t \sigma_\omega^2(t) = \arg\min_t \omega_0(t)\sigma_0^2(t) + \omega_1(t)\sigma_1^2(t) \tag{6}$$

where ω_0 and ω_1 refer to the proportions of the two classes, σ_0^2 and σ_1^2 refer to the variances of the two classes. The resulting image is shown in figure 1(e).

Subsequently, we combine these two binary images of local-to-global thresholding together by morphological conditional dilation to construct the final vessel segmentation, as shown in figure 1(f).

3. Experimental results

3.1. Real and synthetic XCA data

We use real and synthetic XCA data for the experimental evaluation. All the 24 sequences of real XCA data from independent clinical cases are obtained from the Ren Ji Hospital of Shanghai Jiao Tong University. Each sequence contains 80 frames with an image resolution of 512 × 512 pixels with 8 bits per pixel. We manually segmented vessels from the randomly selected vessel frames in corresponding sequences to generate ground truth vessel segmentation for performance evaluation. We randomly selected six typical sequences from these real XCA images as training sets which approximately represent the whole sample space distribution to choose the optimal parameters for our method, while the remaining 18 sequences serve as test sets to evaluate the proposed method. All the experiments were approved by our institutional review board. To accurately evaluate

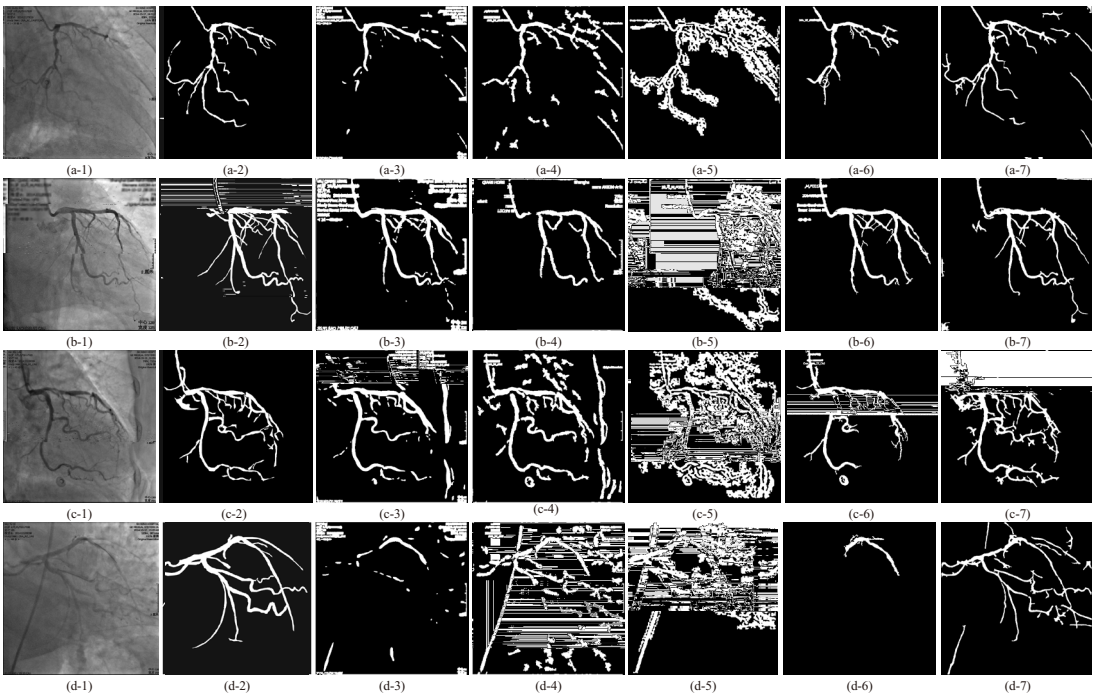

Figure 2.

the vessel segmentation, we construct ten sequences of synthetic XCA images with ground truth background images (GTB) and vessel images (GTV). We perform a vessel extraction described in section 2.3, and remove some residuals manually to obtain the GTVs. The GTBs are consecutive frames selected from the real XCA data. According to the x-ray imaging mechanism (see section 2.2), we multiply a GTV sequence to the clean regions of GTBs from a different sequence to obtain the synthetic XCA data.

3.2. Experiment demonstration

The local window size of the RLF filtering (RLF filtering 2018) is set to 16×16. In order to find the optimal local parameters of Phansalkar thresholding, i.e. p, q, k, we discretize the parameter space in the range $[1, 5]$, $[1, 20]$ and $[0.1, 10]$ respectively, and choose the best parameter values for the best segmentation performance by evaluating the F-measure score introduced in section 3.4. In the training experiments, choosing $p = 3, q = 10, k = 1$ provides the highest F-measure score. The region size threshold t_s in Phansalkar thresholding is set to 300 pixel size. We use the same optimal parameters as in the training experiments to test the proposed method on the test XCA images in subsequent experiments.

To evaluate the segmentation performance, we compared our method with four vessel segmentation algorithms: the Hessian-based Frangi vesselness filter (FrangiFilter) (Frangi *et al* 1998, Hessian-based Frangi vesselness filter 2018), Coye's method (CoyeFilter) (Tyler C 2015), Felfelian's method (Felfelian *et al* 2016) and the MSRG (multiscale region growing) algorithm (Kerkeni *et al* 2016). The parameters of all these five methods are tuned to obtain the best results for all the sequences.

3.3. Visual analysis of the experimental results

The real XCA vessel segmentations are shown in figure 2. Due to the complex backgrounds, all the traditional segmentation methods detect either too few vessels or too much noise with poor performance in recognizing tiny vessels. Considering DECOLOR's ability to detect moving contrasts and the effectiveness of adaptive vessel feature-preserving filtering, the proposed method achieved the most accurate vessel segmentation.

3.4. Quantitative evaluation of vessel segmentation

To quantitatively evaluate the performance of the vessel segmentation, we calculate the detection rate (DR), precision (P) and F-measure (F) using ground truth vessel segmentation. These three indicators are calculated as follows:

$$DR = \frac{TP}{TP + FN}, \quad P = \frac{TP}{TP + FP}, \quad F = \frac{2 * DR * P}{DR + P}, \tag{7}$$

where TP (true positives) is the total number of correctly classified foreground pixels, FP (false positives) is the total number of background pixels that are wrongly marked as foreground, and FN (false negatives) is the total number of foreground pixels that are wrongly marked as background. For a certain method, the detection rate indicates its power to detect more foreground pixels, precision measures the correct ratio of detection, and F-measure combines the detection rate and precision to indicate the overall performance of the certain extractor.

In the real XCA experiments, we manually outlined vessels of 18 images randomly selected from the corresponding different sequences of the test sets as the ground truth for segmentation. Then we measured the detection rate, precision and F-measure shown in figure 3(a). For the synthetic data, the ground truths of all frames are acquired during the synthetic process of the GTVs. However, because the GTBs also contain some vessels, the extracted vessel would inevitably contain more vessels than the GTVs. Therefore, without the ground truth images, we only measured the detection rates of the ten synthetic sequences, as shown in figure 3(b) and table 1.

As can be seen in figure 3(a), though Felfelian's method, which mistakes some backgrounds as foreground vessels, gave the highest DR, it achieved the worst for both precision and F-measure scores. However, the proposed method obtained generally the highest evaluation scores for the real XCA data, and achieved the highest and the most stable performance for synthetic data. Compared to traditional methods, the proposed method can robustly detect the vast majority of the contrast-filled vessel areas.

3.5.

method to achieve superior segmentation performance. This algorithm generally outperforms the state-of-the-art methods.

Acknowledgments

This work was partially supported by the NSFC (61271320) and Shanghai Jiao Tong University Medical Engineering Cross Research Funds (YG2016MS45, YG2015ZD04, YG2014MS29, and YG2014ZD05).

ORCID iDs

Binjie Qin https://orcid.org/0000-0001-7445-1582

References

Ding S *et al* 2010 TIMI myocardial perfusion frame count: a new method to assess myocardial perfusion and its predictive value for short-term prognosis *Catheter. Cardiovasc. Interv.* **75** 722–32

Felfelian B, Fazlali H R, Karimi N, Soroushmehr S M, Samavi S, Nallamothu B and Najarian K 2016 Vessel segmentation in low contrast x-ray angiogram images *Proc. Int. Conf. on Image Processing* vol 2016 pp 375–9

Frangi A F, Niessen W J, Vincken K L and Viergever M A 1998 Multiscale vessel enhancement filtering *Int. Conf. on Medical Image Computing and Computer-Assisted Intervention* pp 130–7

Hensel M, Lundt B, Pralow T and Grigat R R 2016 Robust and fast estimation of signal-dependent noise in medical x-ray image sequences *Bildverarbeitung für die Medizin 2006* (Berlin: Springer) pp 46–50

Hessian-based Frangi vesselness filter www.mathworks.com/matlabcentral/fileexchange/24409 (Accessed: 18 August 2018)

Jin M, Li R, Jiang J and Qin B 2017 Extracting contrast-filled vessels in x-ray angiography by graduated RPCA with motion coherency constraint *Pattern Recognit.* **63** 653–66

Kerkeni A, Benabdallah A, Manzanera A and Bedoui M H 2016 A coronary artery segmentation method based on multiscale analysis and region growing *Comput. Med. Imaging Graph.* **48** 49–61

Kirbas C and Quek F 2004 A review of vessel extraction techniques and algorithms *Comput. Surv.* **36** 81–121

Kitamura Y, Li Y, Ito W I and Ishikawa H 2016 Data-dependent higher-order clique selection for artery vein segmentation by energy minimization *Int. J. Comput. Vis.* **117** 142–58

Kumar R, Vázquez-Reina A and Pfister H 2010 Radon-like features and their application to connectomics *IEEE Computer Society Conf. on Computer Vision and Pattern Recognition Workshops* pp 186–93

Lesage D, Angelini E D, Bloch I and Funka-Lea G 2009 A review of 3D vessel lumen segmentation techniques: models, features and extraction schemes *Med. Image Anal.* **13** 819–45

Liskowski P and Krawiec K 2016 Segmenting retinal blood vessels with deep neural networks *IEEE Trans. Med. Imaging* **35** 2369–80

Ma H, Hoogendoorn A, Regar E, Niessen W J and van Walsum T 2017 Automatic online layer separation for vessel enhancement in x-ray angiograms for percutaneous coronary interventions *Med. Image Anal.* **39** 145–61

Moccia S, Momi E D, Hadji S E and Mattos L S 2018 Blood vessel segmentation algorithms—review of methods, datasets and evaluation metrics *Comput. Methods Programs Biomed.* **158** 71–91

Otsu N 1979 A threshold selection method from gray-level histograms *IEEE Trans. Syst. Man. Cybern. Syst.* **9** 62–6

Phansalkar N, More S, Sabale A and Joshi M 2011 Adaptive local thresholding for detection of nuclei in diversity stained cytology images *Int. Conf. on Communications and Signal Processing* pp 218–20

RLF filtering www.mathworks.com/matlabcentral/fileexchange/27886 (Accessed: 18 August 2018)

Shi C, Cheng Y, Wang J, Wang Y, Mori K and Tamura S 2017 Low-rank and sparse decomposition based shape model and probabilistic atlas for automatic pathological organ segmentation *Med. Image Anal.* **38** 30–49

Syeda-Mahmood T, Wang F, Kumar R, Beymer D, Zhang Y, Lundstrom R and McNulty E 2012 Finding similar 2D x-ray coronary angiograms *Int. Conf. on Medical Image Computing and Computer-Assisted Intervention* pp 501–8

Tang Z, Wu Y W and Fan Y 2017 Groupwise registration of MR brain images with tumors *Phys. Med. Biol.* **62** 6853

Tyler C 2015 A novel retinal blood vessel segmentation algorithm for fundus images *MATLAB Central File Exchange*

Vostatek P, Claridge E, Uusitalo H, Hauta-Kasari M, Fält P and Lensu L 2017 Performance comparison of publicly available retinal blood vessel segmentation methods *Comput. Med. Imaging Graph.* **55** 2–12

Yu C and Sun J 2018 Signal separation from x-ray image sequence using singular value decomposition *Biomed. Sig. Proc. & Control.* **42** 210–5

Zhou X, Yang C and Yu W 2013 Moving object detection by detecting contiguous outliers in the low-rank representation *IEEE Trans. Pattern Anal. Mach. Intell.* **35** 597–610

Zhao Y, Zhao J, Yang J Y, Liu Y, Zhao Y, Zheng Y, Xia L X and Wang Y 2017 Saliency driven vasculature segmentation with infinite perimeter active contour model *Neurocomputing* **259** 201–9

Zhu F, Qin B, Feng W, Wang H, Huang S, Lv Y and Chen Y 2013 Reducing Poisson noise and baseline drift in x-ray spectral images with bootstrap Poisson regression and robust nonparametric regression *Phys. Med. Biol.* **58** 1739